Progress In Electromagnetics Research, PIER 99, 245–260, 2009

EXPLOITATION OF TE-TM SCATTERING DATA FOR MICROWAVE IMAGING THROUGH THE MULTI-SCALING RECONSTRUCTION STRATEGY

L. Poli and P. Rocca

Electromagnetic Diagnostic Laboratory, ELEDIALab
Department of Information Engineering and Computer Science
University of Trento
Via Sommarive 14, Trento 38050, Italy

Abstract—In this paper, the solution of two-dimensional inverse scattering problems is addressed by probing the unknown scenarios with TE and TM waves. To better exploit the information content of the scattered data the multi-zooming approach is used. The results of experiments with single as well as multiple scatterers are reported and discussed also in comparison with single-polarization inversions.

1. INTRODUCTION

Microwave imaging is aimed at reconstructing the geometrical and/or physical properties of unknown objects belonging to an inaccessible domain and probed by a set of known electromagnetic waves. The scattered field data containing the information about the unknown objects are measured outside the domain under test as needed in non-invasive diagnosis (e.g., biomedical imaging [1–8], non-destructive testing [9–12], subsurface archeology [13–15], remote sensing). Besides the kind of material embedded within the investigation domain, the kind of illuminating waves unavoidably influence the field data. Accordingly, it is expected that the use of probing waves having different polarizations can carry out different information. Dealing with two-dimensional inverse scattering problems, the transverse electric (TE) illumination and the transverse magnetic (TM) illumination are usually taken into account. The latter has been more frequently used [16–18] because of the scalar nature of the arising scattering equations. Notwithstanding, the use of TE-polarized

Corresponding author: P. Rocca (paolo.rocca@disi.unitn.it).

incident waves implying the solution of vectorial integral equations have been considered [2, 19–27], as well. Only in few cases, the two data sets have been jointly exploited for inversion procedures. A cascade method where the TE-based and TM-based inversion procedures were performed at successive steps using the result of the first step as initialization of the second one has been described in [28].

This work presents an innovative approach aimed at inverting in a single step the data collected using both TE and TM illuminations. A single cost function exploiting the information related to the z component (i.e., TM polarization) as well as the x, y components (i.e., TE polarization) of the field is optimized through a well known gradient based procedure [29].

To increase the accuracy of the reconstructions, the Iterative Multi-Scaling Approach ($IMSA$) proposed in [30] and successively validated in [31–33] is also applied as a mean for enhancing the data exploitation. As a matter of fact, the $IMSA$ allows a smart allocations of the unknowns within the investigation domain to obtain finer details of the unknown objects as well as to reduce the occurrence of false solutions of local minima of the cost function at hand. At each step of multi-resolution process, a synthetic zoom is performed only within the region where the objects are supposed to be located thanks to the *a-priori* information iteratively gathered from previous steps.

The outline of the paper is as follows. The problem is formulated in Section 2 where the multi-resolution cost function adopted for the retrieval of the unknowns is described, as well. Representative results are reported in Section 3 to assess the effectiveness of the combined $TE + TM$ inversion method. Moreover, comparisons with TM and TE inversion procedures are shown. Eventually, some conclusions are drawn in Section 4.

2. MATHEMATICAL FORMULATION

Let us consider a tomographic two-dimensional scenario where the physical characteristics of the unknown objects are invariant with respect to the z axis. The region under test, called Investigation Domain (D_I), is illuminated by a set of V incident electric fields, $\underline{E}^v_{inc}(x,y)$, $v = 1,\ldots,V$, at a fixed angular frequency, ω. The sources generating the incident field can be either TM polarized [i.e., $\underline{E}^v_{inc}(x,y) = E^v_{inc}(x,y)\,\underline{\hat{z}}$] or TE polarized [i.e., $\underline{E}^v_{inc}(x,y) = E^v_{x,inc}(x,y)\,\underline{\hat{x}} + E^v_{y,inc}(x,y)\,\underline{\hat{y}}$]. In the former case, the interactions between the field and the objects are described through the following

scalar relationship

$$E^v_{z,tot}(x,y) = E^v_{z,inc}(x,y) + k_0^2 \int_{D_I} \tau(x',y') E^v_{z,tot}(x',y') G(x,y|x',y') dx'dy' \quad (1)$$

where $\underline{E}^v_{tot}(x,y) = E^v_{z,tot}(x,y)\,\hat{\underline{z}}$, $v = 1,\ldots,V$, is the total electric field. In (1), the position (x,y) can be either inside D_I or belonging to the measurement domain (D_M) outside D_I. The function $\tau(x,y) = \epsilon_r(x,y) - 1 - j\frac{\sigma(x,y)}{\omega\epsilon_0}$ is the so-called object function, ϵ_r and σ being the relative permittivity and the conductivity, respectively. Moreover, $k_0 = \omega\sqrt{\mu_0\epsilon_0}$ is the free-space wavenumber, ϵ_0 and μ_0 are the background dielectric permittivity and permeability, respectively. The free-space Green's function is $G(x,y|x',y') = -\frac{j}{4}H_0^{(2)}\left(k_0^2\sqrt{(x-x')^2+(y-y')^2}\right)$, $H_0^{(2)}$ being the second kind zero-order Hankel function.

As for the TE illumination, the integral equation is a vectorial one

$$\underline{E}^v_{tot}(x,y) = \underline{E}^v_{inc}(x,y) + \left(k_0^2 + \bigtriangledown\bigtriangledown\cdot\right)\int_{D_I} \tau(x',y')\underline{E}^v_{tot}(x',y')G(x,y|x',y')\,dx'dy'. \quad (2)$$

where the operator $\bigtriangledown$ is applied to the spatial variables.

Integrals (1) and (2) can be also written as

$$\underline{E}^v_{tot}(x,y) = \underline{E}^v_{inc}(x,y) + k_0^2 \int_{D_I} \tau(x',y')\,\underline{E}^v_{tot}(x',y') \cdot \underline{\underline{G}}(x,y|x',y')\,dx'dy' \quad (3)$$

where $\underline{\underline{G}}$ is the dyadic Green's function [21].

Unlike the method proposed in [28], the cost function evaluating the mismatch on the *Data* $[(x,y) \in D_M]$ and *State* $[(x,y) \in D_I]$ terms takes here into account contemporarily all the three components of the electric field. By exploiting the $IMSA$, at each step s of the multi-resolution strategy, a synthetic zooming is performed only within the regions-of-interest (RoIs) where the scatterers have been located at the previous step. Mathematically, the proposed method deals with the following multi-resolution cost function

$$\begin{aligned} &\Phi^{(s)}\left\{\tau\left(x_{n(r)},y_{n(r)}\right),\ E^v_{c,tot}\left(x_{n(r)},y_{n(r)}\right)\right\} = \Phi^{(s)}_{Data} + \Phi^{(s)}_{State} \\ &n(r) = 1,\ldots,N^{(r)};\ r = 0,\ldots,R^{(s)};\ c = x,y,z;\ v = 1,\ldots,V \end{aligned} \quad (4)$$

where

$$\Phi_{Data}^{(s)} = \frac{\sum_{c=x,y,z}\left\{\sum_{v=1}^{V}\sum_{m(v)=1}^{M^{(v)}}\alpha_c \left|E_{scatt}^{c,v}\left(x_{m(v)},y_{m(v)}\right)-\Im_{scatt}^{c,v}\left(x_{m(v)},y_{m(v)}\right)\right|^2\right\}}{\sum_{c=x,y,z}\left\{\sum_{v=1}^{V}\sum_{m(v)=1}^{M^{(v)}}\left|E_{scatt}^{c,v}\left(x_{m(v)},y_{m(v)}\right)\right|^2\right\}} \tag{5}$$

being $E_{scatt}^{c,v}\left(x_{m(v)},y_{m(v)}\right) = E_{tot}^{c,v}\left(x_{m(v)},y_{m(v)}\right) - E_{inc}^{c,v}\left(x_{m(v)},y_{m(v)}\right)$ and

$$\Phi_{State}^{(s)} = \frac{\sum_{c=x,y,z}\left\{\sum_{v=1}^{V}\sum_{r=0}^{R^{(s)}}\sum_{n(r)=1}^{N^{(r)}}\beta_c \left|E_{inc}^{c,v}\left(x_{n(r)},y_{n(r)}\right)-\Im_{inc}^{c,v}\left(x_{n(r)},y_{n(r)}\right)\right|^2\right\}}{\sum_{c=x,y,z}\left\{\sum_{v=1}^{V}\sum_{r=0}^{R^{(s)}}\sum_{n(r)=1}^{N^{(r)}}\left|E_{inc}^{c,v}\left(x_{n(r)},y_{n(r)}\right)\right|^2\right\}} \tag{6}$$

where $R^{(s)} = s-1$, $s = 1,\ldots,S_{opt}$, S_{opt} being the convergence step of the $IMSA$. Moreover, $m(v) = 1,\ldots,M^{(v)}$, $v = 1,\ldots,V$, are the locations of the observation domain where both total and incident fields are measured. Finally, α_c, β_c are real and positive coefficients related to the cth field component.

In (5) and (6), the estimated scattered field $\left[\Im_{scatt}^{c,v}\left(x_{m(v)},y_{m(v)}\right)\right]$ and incident field $\left[\Im_{inc}^{c,v}\left(x_{n(r)},y_{n(r)}\right)\right]$ are computed as follows

$$\Im_{scatt}^{c,v}\left(x_{m(v)},y_{m(v)}\right) = \sum_{r=0}^{R^{(s)}}\sum_{n(r)=1}^{N^{(r)}}\sum_{d=x,y,z}\tau\left(x_{n(r)},y_{n(r)}\right) E_{d,tot}^{v}\left(x_{n(r)},y_{n(r)}\right) G_{cd}\left(x_{n(r)},y_{n(r)}\middle|\, x_{m(v)},y_{m(v)}\right) \tag{7}$$

and

$$\Im_{inc}^{c,v}\left(x_{n(r)},y_{n(r)}\right) = E_{c,tot}^{v}\left(x_{n(r)},y_{n(r)}\right) - \sum_{u(r)=1}^{N^{(r)}}\sum_{d=x,y,z}\tau\left(x_{u(r)},y_{u(r)}\right) E_{d,tot}^{v}\left(x_{u(r)},y_{u(r)}\right) G_{cd}\left(x_{u(r)},y_{u(r)}\middle|\, x_{n(r)},y_{n(r)}\right). \tag{8}$$

To minimize (4), an alternate conjugate-gradient optimization approach is taken into account [29]. Although very effective global optimizers are available (e.g., Genetic Algorithms (GAs) [34–36], Particle Swarm Optimizer (PSO) [37–40], Differential Evolution (DE) [41, 42], Memetic Algorithms (MA) [43, 44], a deterministic approach is used to focus on the "effect" of data on the reconstructions thus avoiding the randomness of stochastic method. The multi-step procedure terminates at $s = S_{opt}$ when the stability conditions, defined in [31] for the TM case, hold true.

3. NUMERICAL ASSESSMENT

In this section, a set of representative results concerned with single and multiple dielectric and lossless ($\sigma = 0$) scatterers are shown. The reconstructions have been carried out starting from noiseless as well as corrupted data. More specifically, the scattered data has been blurred with a random and normally distributed noise having zero mean and standard deviation equal to $\gamma = \frac{\sum_{v=1}^{V}\sum_{m(v)=1}^{M(v)}\left|E_{scatt}^{c,v}\left(x_{m(v)},y_{m(v)}\right)\right|^2}{2MV(SNR)}$, SNR being the signal-to-noise ratio. To evaluate the quality of the reconstructions and to allow a quantitative comparison with the results of the $IMSA-TE$ and $IMSA-TM$ approaches, the following error figure quantifying the mismatch between actual and retrieved object functions has been considered

$$\xi_{(reg)}=\sum_{r=1}^{S_{opt}-1}\frac{1}{N_{(reg)}^{(r)}}\sum_{n_{(r)}=1}^{N_{(reg)}^{(r)}}\left\{\left|\frac{\epsilon_r\left(x_{n(r)},y_{n(r)}\right)-\epsilon_r^{act}\left(x_{n(r)},y_{n(r)}\right)}{\epsilon_r^{act}\left(x_{n(r)},y_{n(r)}\right)}\right|\right\}\times 100. \quad (9)$$

and evaluated within the support of the actual scatterer (i.e., $reg \rightarrow int$), outside the actual scatterer region (i.e., $reg \rightarrow ext$), or on the whole D_I (i.e., $reg \rightarrow tot$).

The first experiment deals with a square homogeneous scatterer characterized by an object function value $\tau^{act} = 0.5$ and belonging to an investigation domain of size $2.4 \times 2.4\lambda_0^2$. The object is off-centered and its center coordinates are $x^{act} = -0.24\lambda_0$, $y^{act} = 0.48\lambda_0$, while the side is $L^{act} = 0.48\lambda_0$. The working frequency is 6 GHz. The field data have been collected at $M^{(v)} = 21$ equally-spaced locations of D_M and a circle $\rho = 1.8\lambda_0$ in radius. $V = 4$ different views, uniformly-spaced around D_I, have been considered. At each iteration, the RoI has been partitioned into $N^{(r)} = 36$ square sub-domains. The same inversion has previously dealt with in [21] through the $IMSA-TE$ method and also compared with the $IMSA-TM$ procedure. Since it has been already proven that for high SNR (e.g., close to noiseless conditions), both $IMSA-TE$ and $IMSA-TM$ reconstruction approaches satisfactorily perform, Fig. 1 reports the inversion results when $SNR = 10$ dB and $SNR = 5$ dB. The $2D$ grey-scale plots show that $IMSA-(TE+TM)$ method improves the other techniques as confirmed by the values of the error indexes in Fig. 2 [$SNR = 10$ dB — Fig. 2(a); $SNR = 5$ dB — Fig. 2(b)]. As a matter of fact, the support of the scatterer is better defined and the reconstructions are more homogeneous without clutters in the background.

The second experiment concerns with a multiple objects scenario. Two off-centered square dielectric objects of side $L_1^{act} = L_2^{act} = 0.67\lambda_0$

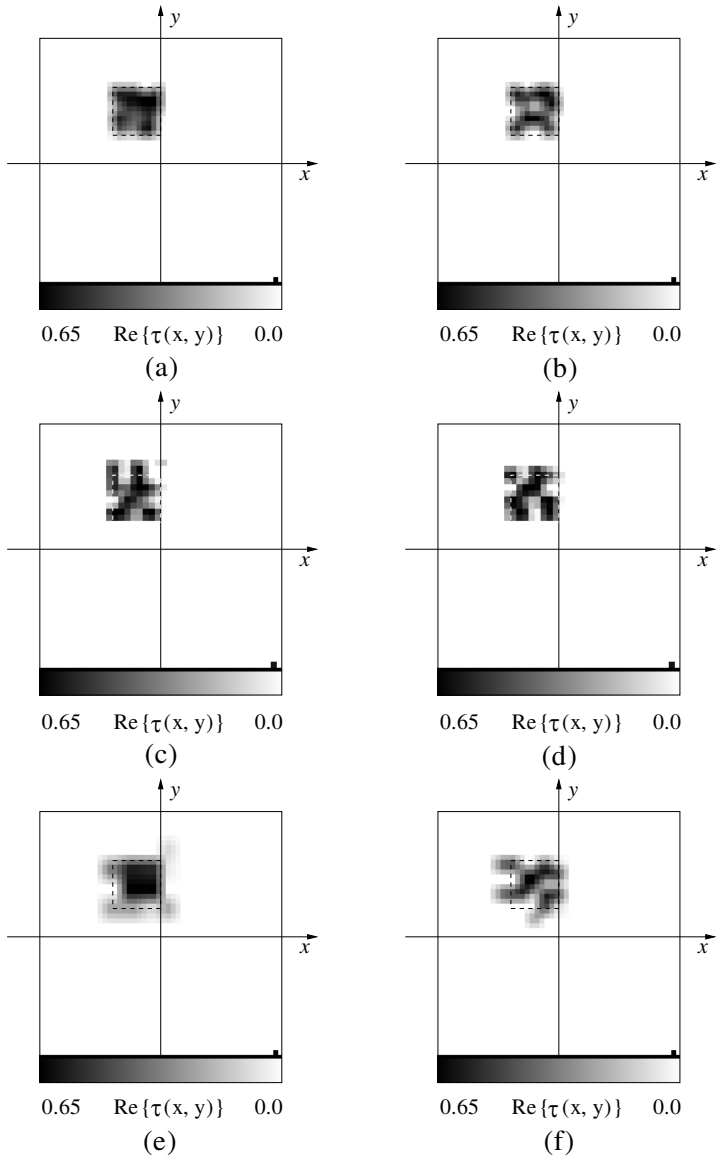

Figure 1. *Single Scatterer* — Reconstruction of the object function with (a)(b) the $IMSA-(TE+TM)$, (c)(d) the $IMSA-TE$, and (e)(f) the $IMSA-TM$ when (a)(c)(e) $SNR=10\,\mathrm{dB}$ and (b)(d)(f) $SNR=5\,\mathrm{dB}$.

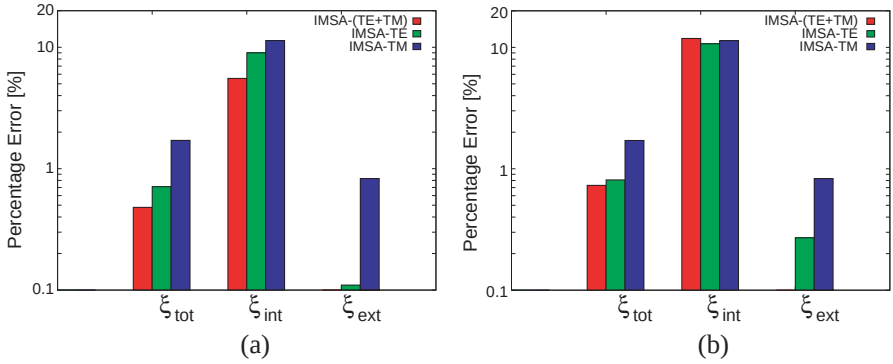

Figure 2. *Single Scatterer. Reconstruction Accuracy* — Behavior of the total (ξ_{tot}), internal (ξ_{int}), and external (ξ_{ext}) errors when (a) $SNR = 10\,\text{dB}$ and (b) $SNR = 5\,\text{dB}$.

are embedded in an investigation domain of dimension $4 \times 4\lambda_0^2$. The objects are homogeneous ($\tau_1^{act} = \tau_2^{act} = 0.5$) and located at $x_1^{act} = y_1^{act} = 0.67\lambda_0$, $x_2^{act} = y_2^{act} = -0.67\lambda_0$ and have side $L_1^{act} = L_2^{act} = 0.67\lambda_0$. The scenario has been probed from $V = 8$ directions by a source working at 4 GHz, while the measurements have been collected at $M^{(v)} = 35$ locations. During the inversion process, the RoI has been partitioned into $N^{(r)} = 100$ cells. Fig. 3 shows the reconstructions obtained with the $IMSA$-based methods. Whether, on one hand, the solutions achieved by the three approaches are quite similar in noiseless conditions, on the other, the performance of the $IMSA-(TE+TM)$ approach are better for noisy scenarios [Figs. 3(d)–3(i)]. As a matter of fact, besides some artifacts in the background also present in both the TE and TM inversions, the profiles of the two scatterers are more accurately estimated by $IMSA-(TE+TM)$. Moreover and likewise the previous example, the values of the object function within the scatterer supports is more uniform especially when processing heavy-noise data (i.e., $SNR = 5\,\text{dB}$). For completeness, the corresponding error figures are given in Fig. 4.

Similar conclusions can be also drawn from the reconstructions in Fig. 5 ($SNR = 5\,\text{dB}$) related to the inversion of two square dielectric objects with different sizes. Such a benchmark problem has been previously considered in [21] where the dielectric distributions in Fig. 5(b) and Fig. 5(c) have been obtained with the $IMSA-TE$ and the $IMSA-TM$, respectively. It is worth noting that the $IMSA-(TE+TM)$ strategy is able to localize both scatterers [Fig. 5(a)] with a higher degree of accuracy, as compared to the other

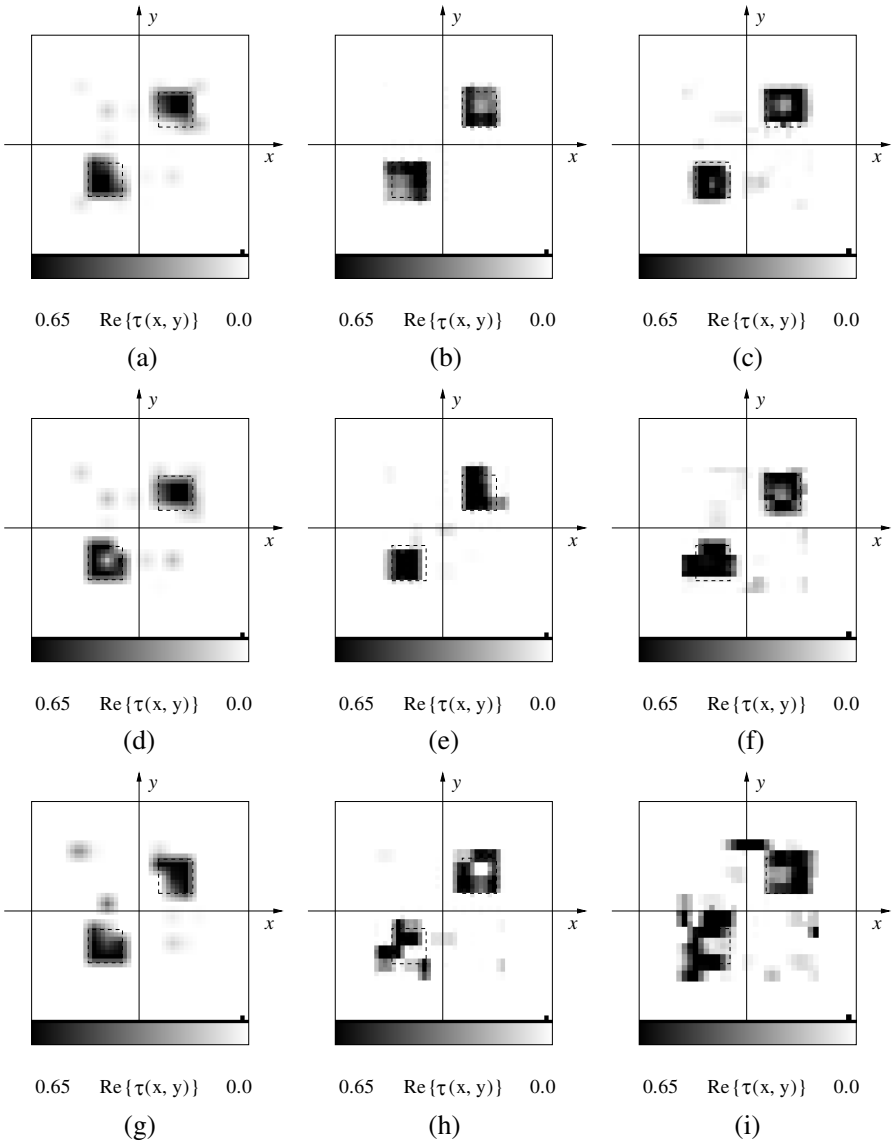

Figure 3. *Two Scatterers* ($L_1^{act} = L_2^{act} = 0.67\lambda_0$) — Reconstruction of the object function with (a)(d)(g) the $IMSA-(TE+TM)$, (b)(e)(h) the $IMSA-TE$, and (c)(f)(i) the $IMSA-TM$ in (a)(b)(c) noiseless condition and when (d)(e)(f) $SNR = 10\,\text{dB}$ and (g)(h)(i) $SNR = 5\,\text{dB}$.

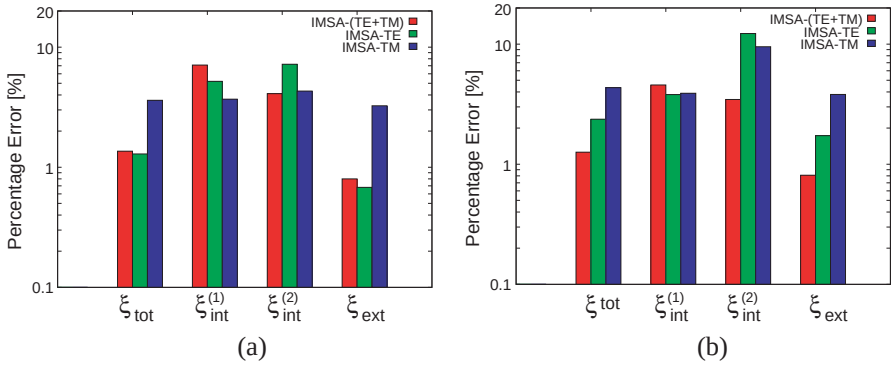

Figure 4. *Two Scatterers* ($L_1^{act} = L_2^{act} = 0.67\lambda_0$). *Reconstruction Accuracy* — Behavior of the total (ξ_{tot}), internal (ξ_{int}), and external (ξ_{ext}) errors when (a) $SNR = 10\,\text{dB}$ and (b) $SNR = 5\,\text{dB}$.

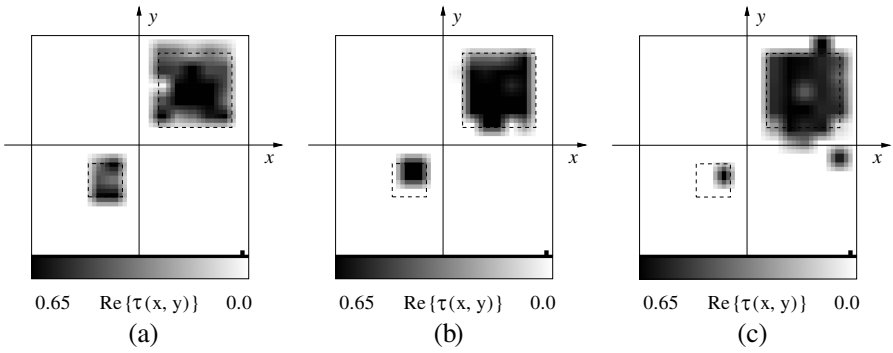

Figure 5. *Two Scatterers* ($L_1^{act} = 0.67\lambda_0$, $L_2^{act} = 1.33\lambda_0$) — Reconstruction of the object function with (a) the $IMSA-(TE+TM)$, (b) the $IMSA-TE$, and (c) the $IMSA-TM$ when $SNR = 5\,\text{dB}$.

algorithms, although the high level of noise. The last experiment considers a more complex scenario. Three homogeneous ($\tau_1^{act} = \tau_2^{act} = \tau_3^{act} = 0.5$) square objects identical in size ($L_i^{act} = 0.67\lambda_0$, $i = \{1, 2, 3\}$) are centered at ($x_1^{act} = y_1^{act} = 0.67\lambda_0$), ($x_2^{act} = -0.67\lambda_0$, $y_2^{act} = 0.67\lambda_0$), and ($x_3^{act} = 0.0$, $y_3^{act} = -0.67\lambda_0$) within a D_I of dimension $4\times4\lambda_0^2$. The illumination frequency has been set to 4 GHz. Moreover, $M^{(v)} = 35$, $v = 1, \ldots, V = 8$, and $N^{(r)} = 100$, $r = 1, \ldots, S_{opt} - 1$. In [21], the $IMSA-TE$ demonstrated an enhanced efficiency compared the $IMSA-TM$ dealing with such an inversion, then hereinafter the comparison is limited to $IMSA-(TE+TM)$ vs. $IMSA-TE$. The solutions in noiseless conditions [Figs. 6(a), 6(b)], when $SNR = 10\,\text{dB}$

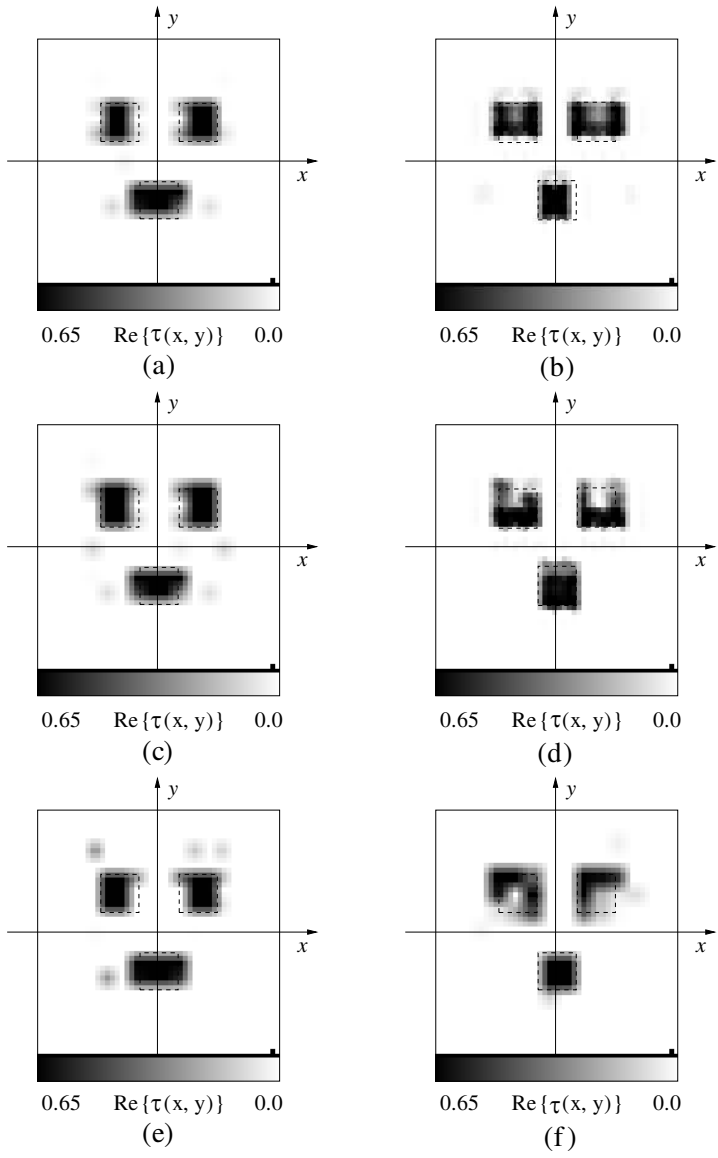

Figure 6. *Three Scatterers* ($L_1^{act} = L_2^{act} = L_3^{act} = 0.67\lambda_0$) — Reconstruction of the object function with (a)(c)(e) the $IMSA-(TE+TM)$ and (b)(d)(f) the $IMSA-TE$ in (a)(b) noiseless condition and when (c)(d) $SNR = 10\,\text{dB}$ and (e)(f) $SNR = 5\,\text{dB}$.

[Figs. 6(c), 6(d)], and $SNR = 5\,\mathrm{dB}$ [Figs. 6(e), 6(f)] are reported. As it can be observed, the three objects are correctly localized within D_I and better resolved by the $IMSA-(TE+TM)$ approach. As a matter of fact, the $IMSA-(TE+TM)$ determines more homogeneous profiles.

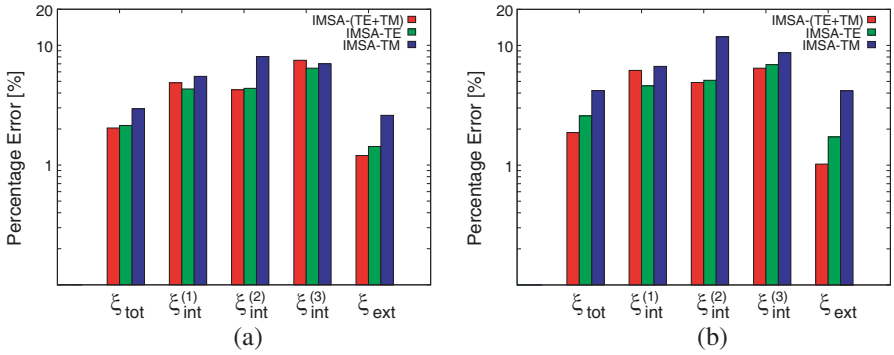

Figure 7. *Three Scatterers* ($L_1^{act} = L_2^{act} = L_3^{act} = 0.67\lambda_0$) — *Reconstruction Accuracy* — Behavior of the total (ξ_{tot}), internal (ξ_{int}), and external (ξ_{ext}) errors when (a) $SNR = 10\,\mathrm{dB}$ and (b) $SNR = 5\,\mathrm{dB}$.

4. CONCLUSIONS

In this paper, the two-dimensional reconstruction of dielectric scatterers illuminated by TE and TM polarized electromagnetic waves has been considered. The field data independently acquired from the two polarizations have been processed by a multi-scaling reconstruction procedure. A set of preliminary results concerned with single and multiple objects as well as noiseless and noisy data have been shown and compared with those from single-polarization inversions.

Such a preliminary assessment has pointed out a potential superior capability of the two-polarization technique that deserves a further and deeper analysis with more complex scatterer distributions and experimental data. Moreover, a thoroughly investigation on the information available from the collected when using different polarization is of interest as well as the possibility to process TM and TE data in a different fashion for designing more efficient inversion procedures. Further investigations will also concern with the use of the same number of equations in the inversion procedures when dealing with noisy scenarios for the case of independent and identically distributed noise. As a matter of fact, three noisy measurements per

receiver with the TM antennas could reduce the noise variance in the reconstructions.

Notwithstanding, since generally different antennas are used to collect TE or TM polarization data, the engineering problems related to the collection of both polarizations deserve a deeper analysis. For example, the evaluation of whether it is more advantageous to either use the same number of antennas for TE and TM measurements, or favor the use of more antennas of a certain polarization over the other one has to be faced.

REFERENCES

1. Caorsi, S., A. Massa, and M. Pastorino, "Numerical assessment concerning a focused microwave diagnostic method for medical applications," *IEEE Trans. Antennas Propag.*, Vol. 48, No. 11, 1815–1830, Nov. 2000.
2. Abubakar, A., P. M. Van Den Berg, and J. J. Mallorqui, "Imaging of biomedical data using a multiplicative regularized contrast source inversion method," *IEEE Trans. Microw. Theory Tech.*, Vol. 50, No. 7, 1761–1771, Jul. 2002.
3. Caorsi, S., A. Massa, M. Pastorino, and A. Rosani, "Microwave medical imaging: Potentialities and limitations of a stochastic optimization technique," *IEEE Trans. Microw. Theory Tech.*, Vol. 52, No. 8, 1909–1916, Aug. 2004.
4. Bindu, G., A. Lonappan, V. Thomas, C. K. Aanandan, and K. T. Mathew, "Dielectric studies of corn syrup for applications in microwave breast imaging," *Progress In Electromagnetics Research*, PIER 59, 175–186, 2006.
5. Bindu, G., S. J. Abraham, A. Lonappan, V. Thomas, C. K. Aanandan, and K. T. Mathew, "Active microwave imaging for breast cancer detection," *Progress In Electromagnetics Research*, PIER 58, 149–169, 2006.
6. Benedetti, M., M. Donelli, A. Martini, M. Pastorino, A. Rosani, and A. Massa, "An innovative microwave imaging technique for non-destructive evaluation: Applications to civil structures monitoring and biological bodies inspection," *IEEE Trans. Instrum. Meas.*, Vol. 55, No. 6, 1878–1884, Dec. 2006.
7. Zhang, H., S. Y. Tan, and H. S. Tan, "A novel method for microwave breast cancer detection," *Progress In Electromagnetics Research*, PIER 83, 413–434, 2008.
8. Zhou, H., T. Takenaka, J. Johnson, and T. Tanaka, "A breast imaging model using microwaves and a time domain three dimen-

sional reconstruction method," *Progress In Electromagnetics Research*, PIER 93, 57–70, 2009.

9. Weedon, W. H., W. C. Chew, and P. E. Mayes, "A step-frequency radar imaging system for microwave nondestructive evaluation," *Progress In Electromagnetics Research*, PIER 28, 121–146, 2000.
10. Pastorino, M., S. Caorsi, and A. Massa, "A global optimization technique for microwave nondestructive evaluation," *IEEE Trans. Instrum. Meas.*, Vol. 51, No. 4, 666–673, Aug. 2002.
11. Benedetti, M., M. Donelli, G. Franceschini, M. Pastorino, and A. Massa, "Effective exploitation of the a-priori Information through a microwave imaging procedure based on the SMW for NDE/NDT applications," *IEEE Trans. Geosci. Remote Sens.*, Vol. 43, No. 11, 2584–2592, Nov. 2005.
12. Thomas, V., J. Yohannan, A. Lonappan, G. Bindu, and K. T. Mathew, "Localization of the investigation domain in electromagnetic imaging of buried 2-D dielectric pipelines with circular cross section," *Progress In Electromagnetics Research*, PIER 61, 111–131, 2006.
13. Bermani, E., S. Caorsi, and M. Raffetto, "An inverse scattering approach based on a neural network technique for the detection of dielectric cylinders buried in a lossy half-space," *Progress In Electromagnetics Research*, PIER 26, 67–87, 2000.
14. Benedetti, M., M. Donelli, G. Franceschini, M. Pastorino, and A. Massa, "Evaluation study of the effectiveness of the integrated GA-based strategy for the tomographic subsurface detection of defects," *J. Opt. Soc. America A*, Vol. 23, No. 6, 1311–1325, 2006.
15. Li, F., X. Chen, and K. Huang, "Microwave imaging a buried object by the GA and using the S_{11} parameter," *Progress In Electromagnetics Research*, PIER 85, 289–302, 2008.
16. Azaro, R., A. Casagranda, D. Franceschini, and A. Massa, "An innovative fuzzy-logic-based strategy for an effective exploitation of noisy inverse scattering data," *Progress In Electromagnetics Research*, PIER 54, 283–302, 2005.
17. Chien, W., "Inverse scattering of an un-uniform conductivity scatterer buried in a three-layer structure," *Progress In Electromagnetics Research*, PIER 82, 1–18, 2008.
18. Huang, C.-H., C.-C. Chiu, C.-L. Li, and K.-C. Chen, "Time domain inverse scattering of a two-dimensional homogenous dielectric object with arbitrary shape by particle swarm optimization," *Progress In Electromagnetics Research*, PIER 82, 381–400, 2008.

19. Joachimowicz, N., C. Pichot, and J.-P. Hugonin, "Inverse scattering: An iterative numerical method for electromagnetic imaging," *IEEE Trans. Antennas Propag.*, Vol. 39, No. 12, 1742–1752, Dec. 1991.
20. Chiu, C.-C. and C. J. Lin, "Image reconstruction of buried dielectric cylinders by TE wave illumination," *Progress In Electromagnetics Research*, PIER 34, 271–284, 2001.
21. Franceschini, D., M. Donelli, G. Franceschini, and A. Massa, "Iterative image reconstruction of two-dimensional scatterers illuminated by TE waves," *IEEE Trans. Microw. Theory Tech.*, Vol. 51, No. 4, 1162–1173, Apr. 2003.
22. Azaro, R., M. Donelli, D. Franceschini, and A. Massa, "Multiscaling reconstruction of metallic targets from TE and TM experimental data," *Microw. Opt. Tech. Lett.*, Vol. 48, No. 2, 322–324, Feb. 2006.
23. Uno, T. and S. Adachi, "Inverse scattering method for one-dimensional inhomogeneous layered media," *IEEE Trans. Antenna Propag*, Vol. 35, No. 12, 1456–1466, Dec. 1987.
24. Cui, T. J. and C. H. Liang, "Inverse scattering method for one-dimensional inhomogeneous lossy medium by using a microwave networking technique," *IEEE Trans. Microw. Theory Tech.*, Vol. 43, No. 8, 1773–1781, Aug. 1995.
25. Ma, J., W. C. Chew, C.-C. Lu, and J. Song, "Image reconstruction from TE scattering data using equation of strong permittivity fluctuation," *IEEE Trans. Antennas Propag.*, Vol. 48, No. 6, 860–867, Jun. 2000.
26. Lin, Y.-S., C.-C. Chiu, and Y.-C. Chen, "Image reconstruction for a perfectly conducting cylinder buried in a three-layer structure by TE wave illumination," *Proc. Int. Conf. Computational Electromagnetics Applications (ICCEA 2004)*, 411–414, Nov. 1–4, 2004.
27. Hajihashemi, M. R. and M. El-Shenawee, "TE Versus TM for the shape reconstruction of 2-D PEC targets using the Level-Set algorithm," *IEEE Trans. Geosci. Remote Sens.*, in press, 2009.
28. Chou, C.-P. and Y.-W. Kiang, "Inverse scattering of dielectric cylinders by a cascade TE-TM method," *IEEE Trans. Microw. Theory Tech.*, Vol. 47, No. 10, 1923–1930, Oct. 1999.
29. Kleinmann, R. E. and P. M. Van den Berg, "A modified gradient method for two-dimensional problems in tomography," *J. Comput. Appl. Math.*, Vol. 42, No. 1, 17–35, 1992.
30. Caorsi, S., M. Donelli, D. Franceschini, and A. Massa, "A new

methodology based on an iterative multiscaling for microwave imaging," *IEEE Trans. Microw. Theory Tech.*, Vol. 51, No. 4, 1162–1173, Apr. 2003.

31. Caorsi, S., M. Donelli, and A. Massa, "Detection, location and imaging of multiple scatterers by means of the iterative multiscaling method," *IEEE Trans. Microw. Theory Tech.*, Vol. 52, No. 4, 1217–1228, Apr. 2004.
32. Caorsi, S., M. Donelli, and A. Massa, "Analysis of the stability and robustness of the iterative multi-scaling approach for microwave imaging applications," *Radio Sci.*, Vol. 39, 1–17, Oct. 2004.
33. Donelli, M., D. Franceschini, G. Franceschini, and A. Massa, "Effective exploitation of multi-view data through the iterative multi-scaling method — An experimental assessment," *Progress In Electromagnetics Research*, PIER 54, 137–154, 2005.
34. Pastorino, M., A. Massa, and S. Caorsi, "A microwave inverse scattering technique for image reconstruction based on a genetic algorithm," *IEEE Trans. Instrum. Meas.*, Vol. 49, No. 3, 573–578, Jun. 2000.
35. Caorsi, S., A. Massa, and M. Pastorino, "A computational technique based on a real-coded genetic algorithm for microwave imaging purposes," *IEEE Trans. Geosci. Remote Sens.*, Vol. 38, No. 4, 1697–1708, Jul. 2000.
36. Massa, A., D. Franceschini, G. Franceschini, M. Raffetto, M. Pastorino, and M. Donelli, "Parallel GA-based approach for microwave imaging applications," *IEEE Trans. Antennas Propag.*, Vol. 53, No. 10, 3118–3127, Oct. 2005.
37. Caorsi, S., M. Donelli, A. Lommi, and A. Massa, "Location and imaging of two-dimensional scatterers by using a particle swarm algorithm," *Journal of Electromagnetic Waves and Applications*, Vol. 18, No. 4, 481–494, 2004.
38. Donelli, M. and A. Massa, "A computational approach based on a particle swarm optimizer for microwave imaging of two-dimensional dielectric scatterers," *IEEE Trans. Microw. Theory Tech.*, Vol. 53, No. 5, 1761–1776, May 2005.
39. Donelli, M., G. Franceschini, A. Martini, and A. Massa, "An integrated multi-scaling strategy based on a particle swarm algorithm for inverse scattering problems," *IEEE Trans. Geosci. Remote Sens.*, Vol. 44, No. 2, 298–312, Feb. 2006.
40. Semnani, A. and M. Kamyab Hesari, "Truncated cosine fourier series expansion method for solving 2-D inverse scattering problems," *Progress In Electromagnetics Research*, PIER 81, 73–97, 2008.

41. Massa, A., M. Pastorino, and A. Randazzo, "Reconstruction of two-dimensional buried objects by a hybrid differential evolution method," *Inverse Problems*, Vol. 20, No. 6, 135–150, Dec. 2004.
42. Rekanos, I. T., "Shape reconstruction of a perfectly conducting scatterer using differential evolution and particle swarm optimization," *IEEE Trans. Geosci. Remote Sens.*, Vol. 46, No. 7, 1967–1974, Jul. 2008.
43. Caorsi, S., A. Massa, M. Pastorino, M. Raffetto, and A. Randazzo, "Detection of buried inhomogeneous elliptic cylinders by a memetic algorithm," *IEEE Trans. Antennas Propag.*, Vol. 51, No. 10, 2878–2884, Oct. 2003.
44. Caorsi, S., A. Massa, M. Pastorino, and A. Randazzo, "Electromagnetic detection of dielectric scatterers using phaseless synthetic and real data and the memetic algorithm," *IEEE Trans. Geosci. Remote Sens.*, Vol. 41, No. 12, 2745–2753, Dec. 2003.